Available online at www.sciencedirect.com
SCIENCE DIRECT®
International Journal of Heat and Mass Transfer 48 (2005) 2583–2592
International Journal of HEAT and MASS TRANSFER
www.elsevier.com/locate/ijhmt

Study on the transient characteristics of the sensor tube of a thermal mass flow meter

Il Young Han, Dong-Kwon Kim, Sung Jin Kim *

Department of Mechanical Engineering, Korea Advanced Institute of Science and Technology, Taejon 305-701, Korea

Received 5 May 2004; received in revised form 17 January 2005

Abstract

In the present work, a simple numerical model for transient heat transfer phenomena involving the sensor tube of a thermal mass flow meter (TMFM) is presented. In order to validate the proposed model, extensive experimental investigations are performed. Based on the results of the proposed model, the transient heat transfer mechanism in the sensor tube is explained. Finally, a correlation for predicting the response time of the sensor tube is presented. This correlation can estimate the response time of the sensor tube quantitatively with errors of less than 30%. By using the proposed correlation, physical meanings and characteristics of the response time of the sensor tube are presented.

1. Introduction

The measurement and control of gas flow rates is critical in many engineering applications, including semiconductor manufacturing processes and chemical processes. The general flow detection methods are orifice, turbine, ultrasonic, coriolis and MEMS flow sensors [1–4]. Specifically, in the semiconductor and chemical industry, thermal mass flow meters (TMFMs) are most widely used for measuring mass flow rates [5]. A TMFM typically consists of a sensor tube, a bypass (main) tube, and electric circuits, as shown in Fig. 1. A sensor tube in a TMFM is a long, slender stainless steel capillary tube with heating and temperature-sensing wires wrapped around it [6]. There are several types of sensor tubes, which vary in the number and configuration of heaters and sensors used [7–10]. In a conventional TMFM, a single heater is centered on the sensor tube, and two temperature-sensitive resistors are placed symmetrically at the upstream and downstream sides of the heater, as shown in Fig. 2 [11]. The working principle is schematically explained in Fig. 2. When electric power is applied to the heater, the temperature profile on the sensor tube is symmetric at zero flow rate. When a gas flows through the sensor tube, the upstream temperature sensor is cooled by the gas flow, and the downstream temperature sensor is heated by the gas which was preheated in the upstream section. The temperature difference between the two temperature sensors increases with increasing flow rate. This allows for measurement of the flow rate through the sensing of the temperature difference.

A TMFM should have a short response time in order to measure the time-varying flow rate rapidly and accurately. Thus, it is important to study transient heat transfer phenomena for the sensor tube of a TMFM. The response time of the sensor tube is a dominant

* Corresponding author. Tel.: +82 42 869 3043; fax: +82 42 869 8207.
E-mail address: sungjinkim@kaist.ac.kr (S.J. Kim).

0017-9310/$ - see front matter © 2005 Elsevier Ltd. All rights reserved.
doi:10.1016/j.ijheatmasstransfer.2005.01.021

Nomenclature

A	cross-sectional area, m^2
C	heat capacity, J/kg K
D_{in}	inner diameter of the tube, m
D_{out}	outer diameter of the tube, m
h_i	interstitial heat transfer coefficient, W/m^2 K
k	thermal conductivity, W/m K
L	length of the tube, m
L_h	heating length, m
L_s	distance from the center of the sensor tube to the sensor, m
$\dot{m}$	mass flow rate of the fluid, kg/s
Nu_i	interstitial Nusselt number
P	wetted perimeter of the tube, m
q	rate of heat flow, W
q'	heat flux per unit length applied to the tube, W/m
q'_{tf}	heat flux per unit length from the tube to the fluid, W/m
q''	heat flux, W/m^2
R	inner radius of the sensor tube, m
R_r	thermal resistance per unit length for radial heat loss, m K/W
t	time, s
t_{final}	time at the final steady state, s
t_{resp}	response time, s
T	characteristic temperature, K
$\overline{T}$	average temperature, K
U_{mean}	mean velocity, m/s
x	axial coordinate

Greek symbol

ρ	density, kg/m^3

Superscripts

U	upstream side of the sensor tube
D	downstream side of the sensor tube

Subscripts

amb	ambient
f	fluid
F	final steady state
I	initial state
t	tube
T	transient state

factor for the response time of a TMFM, because the sensor tube has a sluggish response time compared to other electronic components of a TMFM. Therefore, the response time of the sensor tube is a critical part of the overall design of a TMFM.

The investigation of TMFMs was initiated by Tomas [7]. Since then, there has been a great deal of research conducted with models of various complexity for analyzing heat transfer phenomena in sensor tubes. Komiya et al. [12] presented a one-dimensional steady-state solution. They neglected radial temperature variation and axial conduction within the fluid in the sensor tube. They also assumed constant heating conditions along the sensor tube in order to simplify the problem. Rudent and Navratil [6] presented an analytic model considering thermal interaction between the sensor tube and the fluid, taking into account the temperature difference between the two. Recently, Kim and Jang [13] conducted numerical and experimental investigations under steady-state conditions in order to fully understand

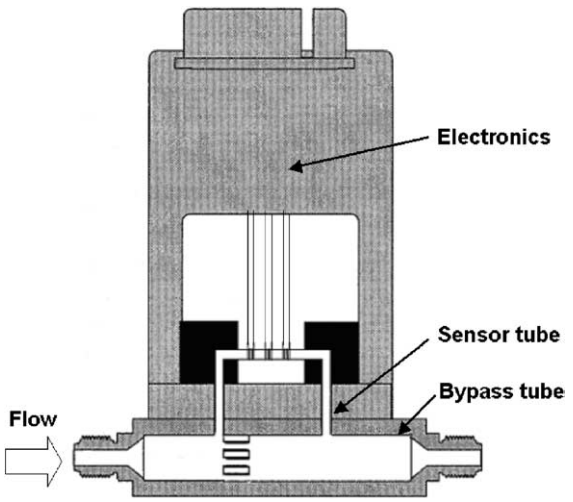

Fig. 1. Schematic diagram of a TMFM.

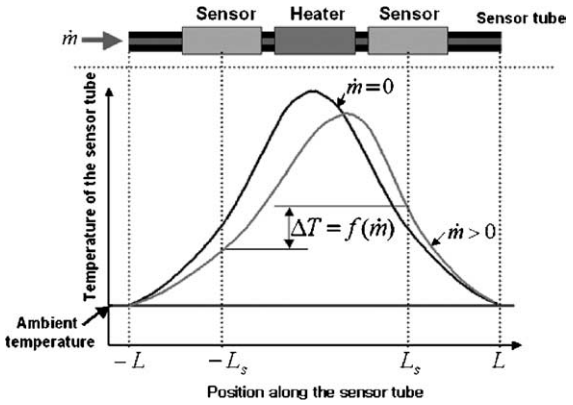

Fig. 2. Schematic layout of the sensor tube.

heat-transfer interactions between the sensor tube and the fluid. Even though many models have been presented by previous investigators, most of them focused on steady-state heat transfer phenomena [6,7,12–14]. There have been only a few studies focusing on the analysis of the transient heat transfer phenomena in sensor tubes [11,15], and these were limited to qualitative evaluation. Therefore, to the authors' knowledge, there is no reliable data or correlation by which one can predict the response time of a sensor tube quantitatively.

The present study is devoted to numerical modeling of the transient thermal performance of a sensor tube and the quantitative prediction of the response time. Thus, we present a simple numerical model for a transient heat transfer process in a sensor tube. An experimental investigation is also conducted to provide experimental data, which are used for validating the proposed model. Based on the results of the simple model, the transient heat transfer mechanism in the sensor tube is explained. Finally, a correlation for predicting the response time of a sensor tube is presented using the simple model. Using this correlation, the physical meaning and characteristics of the response time of the sensor tube are presented.

2. Numerical analysis methods

This work deals with transient heat transfer phenomena in the sensor tube. The schematic diagram of a physical model of the sensor tube is shown in Fig. 3. Constant power is supplied to a central region of the sensor tube. Heat flux per unit length applied to the sensor tube is given as

$$q' = \begin{cases} q'_0 & (-L_h \leqslant x \leqslant L_h) \\ 0 & (x < -L_h, x > L_h) \end{cases} \tag{1}$$

where L_h is the heating length. There is no fluid flow in the sensor tube until $t = 0$, and a fluid suddenly flows with a constant volume flow rate through the sensor tube for $t > 0$.

$$\dot{m} = \begin{cases} 0 & (t < 0) \\ \dot{m}_0 & (t \leqslant 0) \end{cases} \tag{2}$$

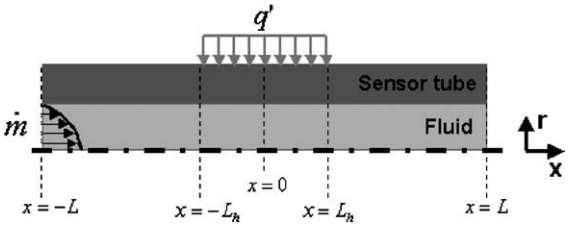

Fig. 3. Schematic diagram of a physical model.

In analyzing transient heat transfer phenomena in the sensor tube, the flow is assumed to be laminar and hydrodynamically fully developed. As the full-scale range of the gas flow that can be measured in the sensor tube is typically limited to low mass flow rates, the maximum flow rate through the sensor tube in the present research is chosen to be 50 SCCM (standard cubic centimeters per minute) [11]. The Reynolds number at the maximum mass flow rate is 107 for a 0.8-mm outer diameter tube. Hence, the flow in the sensor tube can be safely assumed to be laminar. The hydrodynamic entry length of the tube required for development of the laminar velocity profile is calculated to be 4.3 mm [16]. Because the hydrodynamic entry length is much smaller than the total length of the sensor tube, the flow in the sensor tube can be considered as a fully developed Poiseuille flow in a circular tube. The velocity profile in the sensor tube is given as

$$u = 2U_{\text{mean}}\left(1 - \frac{r^2}{R^2}\right) \tag{3}$$

where U_{mean} and R are mean velocity and the inner radius of the sensor tube. We also assume heat is lost due only to radiation from the outer surface of the sensor tube as in a vacuum. Below we present two methods for obtaining the temperature distributions in the fluid and the solid wall. The first method is the conventional approach, in which the two-dimensional energy equation is solved numerically in the fluid and solid regions. We propose the second method as an improvement to the conventional approach. In this method, two simplified energy equations are obtained by taking averages of the solid and fluid temperatures in the radial direction.

2.1. Two-dimensional numerical model

Transient heat transfer phenomena in the sensor tube are analyzed using a two-dimensional numerical model. The temperature field in the gas as well as in the tube wall is governed by the following energy equation.

$$\rho C_P \frac{\partial T}{\partial t} + \rho C_P u \frac{\partial T}{\partial x} = \frac{1}{r}\frac{\partial}{\partial r}\left(k \cdot r \frac{\partial T}{\partial r}\right) + \frac{\partial}{\partial x}\left(k \frac{\partial T}{\partial x}\right) \tag{4}$$

where u, k, ρ, C_p, and T are axial velocity, thermal conductivity, gas density, specific heat of the gas, and temperature, respectively. The boundary conditions needed to solve the governing equations are given as follows.

$$T(x = -L) = T_{\text{amb}} \tag{5}$$

$$T(x = L, r > R) = T_{\text{amb}} \tag{6}$$

$$\left[\rho C_P \frac{\partial T}{\partial t} + \rho C_P u \frac{\partial T}{\partial x} - \frac{1}{r}\frac{\partial}{\partial r}\left(k \cdot r \frac{\partial T}{\partial r}\right)\right]_{x=L, r \leqslant R} = 0 \tag{7}$$

The temperatures at both ends of the tube are assumed to be ambient temperature [6,12]. Patankar's suggestion [17] for the outflow boundary condition is adopted. Governing equations are solved by the control-volume-based finite difference method. A power law scheme is used for discretization of the conduction and convection terms. A fully implicit scheme is used for discretizaition of the unsteady terms. Discretization equations are calculated by the ADI method which was introduced by Peaceman and Rachford [18].

The two-dimensional numerical model is a conventional approach to analyze the transient heat transfer phenomena in the sensor tube. However, this model requires a lot of time and computing power. In addition, it is not easy to identify the important parameters that affect the transient characteristics in the sensor tube. Therefore, we propose a simplified model to overcome the demerits of the two-dimensional numerical model.

2.2. One-dimensional numerical model

We use an averaging technique on the two-dimensional governing equations in order to reduce the amount of computation required. The physical domain can be divided into two regions separated by a circular cylinder with a radius equal to the inner radius of the sensor tube. One is a sensor tube region, and the other is a fluid region. So, there are two governing equations for the sensor tube and fluid temperatures averaged in the radial direction. The energy balance for the sensor tube region and the inner fluid is represented by

$$k_t A_t \overline{T}_t'' + h_i P(\overline{T}_f - \overline{T}_t) - \frac{1}{R_r}(\overline{T}_t - T_{amb}) + q' = A_t \rho_t C_t \frac{\partial \overline{T}_t}{\partial t} \tag{8}$$

$$k_f A_f \overline{T}_f'' - \dot{m} C_f \overline{T}_f' + h_i P(\overline{T}_t - \overline{T}_f) = A_f \rho_f C_f \frac{\partial \overline{T}_f}{\partial t} \tag{9}$$

where $\overline{T}$, h_i and q' are average temperature, interstitial heat transfer coefficient and heat flux per unit length supplied from the heater, respectively. The first term on the left-hand side of Eq. (8) is the axial conduction term, and the second term implies thermal interaction between the sensor tube and the fluid. The third term accounts for a radial heat loss from the outer wall of the tube to the surroundings. There is a transient term on the right-hand side of Eq. (8). Similarly, Eq. (9) consists of the conduction term in the axial direction, the enthalpy change term of the fluid, the thermal interaction term, and the transient term. In Eqs. (8) and (9), the averaged values are used for the tube and fluid temperatures. Boundary conditions are basically the same as those for the two-dimensional numerical model.

$$\overline{T}_t(x = -L) = T_{amb} \tag{10}$$

$$\overline{T}_t(x = L) = T_{amb} \tag{11}$$

$$\overline{T}_f(x = -L) = T_{amb} \tag{12}$$

$$\left[-\dot{m} C_f \overline{T}_f' + h_i P(\overline{T}_t - \overline{T}_f) - A_f \rho_f C_f \frac{\partial \overline{T}_f}{\partial t}\right]_{x=L} = 0 \tag{13}$$

The simple numerical model is presented with the interstitial heat transfer coefficient h_i. It is given as

$$h_i = \frac{q_{tf}'}{(\overline{T}_s - \overline{T}_f)} \tag{14}$$

where q_{tf}' is heat transfer rate per unit length from the tube to the fluid. As shown in Eq. (14), h_i is calculated with an average (arithmetic mean) temperature of the fluid instead of the bulk mean temperature of the fluid. We need to know the value of the interstitial heat transfer coefficient h_i in order to solve the simple model of Eqs. (8) and (9). Thus we use the two-dimensional numerical model to predict the interstitial heat transfer coefficient. Fig. 4 shows the results of the two-dimensional numerical model. The interstitial Nusselt number is generally defined as

$$Nu_i = \frac{h_i D_{in}}{k_f} \tag{15}$$

where D_{in} is the inner diameter of the sensor tube. As can be seen from Fig. 4, it is reasonable to use 6 as an approximate value for the interstitial Nusselt number. Using this approximation, the results of the simple numerical model agree closely with the two-dimensional numerical model, as shown in Fig. 5.

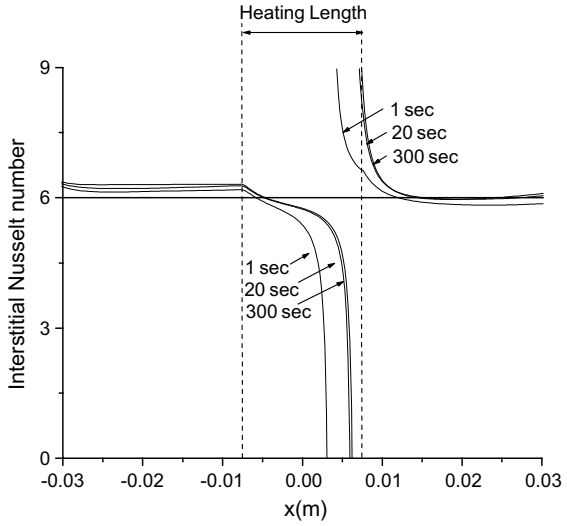

Fig. 4. Interstitial Nusselt numbers at a transient state.

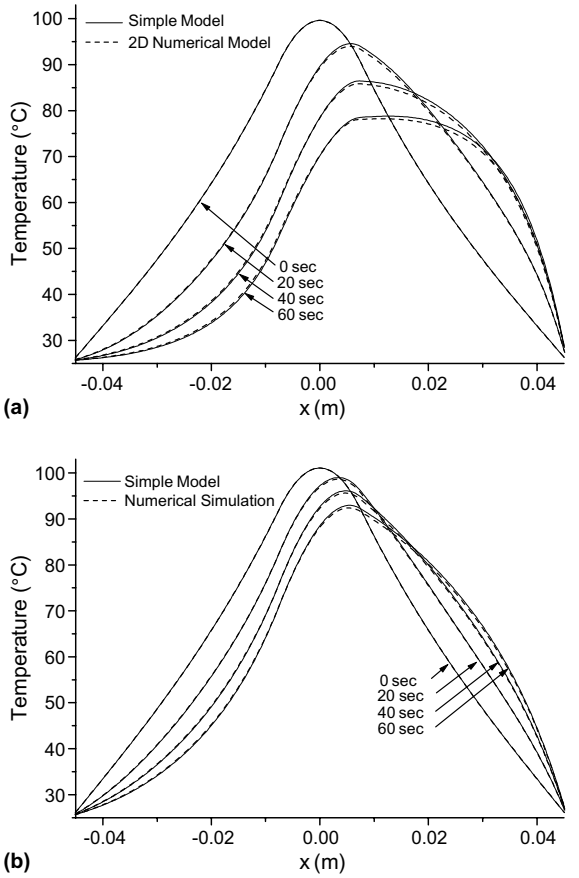

Fig. 5. Comparison between tube-wall temperature profiles using the simple numerical model and conventional 2-D numerical model for a mass flow rate of 30 SCCM. (a) When the outer diameter is 0.8 mm. (b) When the outer diameter is 1.2 mm.

3. Experimental validation

An experimental investigation was performed to validate the proposed numerical model. The experimental apparatus is shown schematically in Fig. 6. The nitrogen gas passes through a capillary tube made of stainless steel 304 which has a length of 91 mm. The nitrogen gas is used in the present experiment because typical TMFMs currently employed in semiconductor fabrication processes are calibrated with nitrogen gas. As shown in Table 1, we used capillaries with several inner and outer diameters. The heating wire wound around the tube is made of a nickel–chromium alloy (Ni: 80%, Cr: 20%), the resistivity of which is independent of the temperature variations. The heater is powered by a DC power supply manufactured by Hewlett Packard. The sensor housing is connected to a vacuum chamber. This chamber is evacuated by a mechanical pump and an oil diffusion pump in order to eliminate the heat loss due to conduction and convection from the sensor tube. Because a pressure below 10^{-4} Torr suppresses the natural convection and conduction around the sensor tube completely [15], we can estimate the heat loss by radiation only. The gas flows into the sensor tube from a pressure tank through a metering valve and a solenoid valve. The metering valve is used for setting the volume flow rate. The flow rate of gas is measured by a pre-calibrated TMFM on the downstream side of the sensor tube. This TMFM is Brooks Instrument model 5850. The uncertainty of the TMFM in the range of these experiments is ±1%. We conducted experiments over the flow range of 0 to 50 SCCM (standard cubic centimeters per minute). Nine thermocouples are attached to the outer surface of the sensor tube to measure wall temperature distributions. We used K-type miniature thermocouple wires with a diameter of 0.0125 mm, which are manufactured by OMEGA Engineering. The diameter of the thermocouple wire is small enough to neglect conduction through it. The positions of thermocouples for temperature measurement are shown in Fig. 7. The temperature signals were recorded from the start of gas flow through the sensor tube by suddenly opening the solenoid valve attached in the upstream section of the sensor tube. The response time of the solenoid valve is less than 0.1 s. It does not affect the response time of the sensor tube, because the latter is generally from 10 to 30 s. The measured voltage signals were acquired using a Hewlett-Packard E1326B digital multi-meter and converted into temperatures using Agilent's VEE data acquisition and reduction software [19]. In obtaining the experimental results, we conducted experiments 5 times.

To analyze the signal errors, we conducted an uncertainty analysis. The measurement error consists of bias error and precision error. The uncertainty U is given as follows [20].

$$U = (B^2 + P^2)^{1/2} \tag{16}$$

where B and P are bias uncertainty and precision uncertainty, respectively. The precision uncertainty is determined by

$$P = t_{95\%,v}\frac{S}{\sqrt{N}} \tag{17}$$

$$v = N - 1, S = \sqrt{\frac{1}{N}\sum_{i=1}^{N}(x_i - \bar{x})^2}$$

where $t_{95\%,v}$, S, v, N, $\bar{x}$ and x_i are t-distribution for a confidence level of 95%, standard deviation, degree of freedom, data number, sample mean and measured value of a particular experiment.

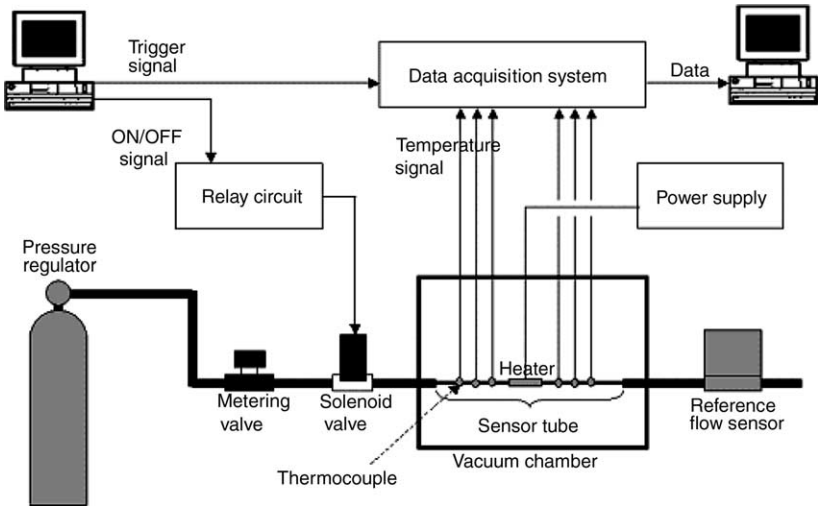

Fig. 6. Schematic diagram of the total experimental apparatus.

Table 1
Inner and outer diameters of sensor tubes

Number	Outer diameter (mm)	Inner diameter (mm)
1	1.257	0.977
2	0.812	0.562

4. Transient thermal characteristics of a sensor tube

Figs. 8 and 9 show the transient temperature profiles for the sensor tube of 0.8 mm outer diameter and the sensor tube of 1.2 mm outer diameter, respectively. As can be seen from these figures, the results from the simple numerical model are in close agreement with the experimental results. The tube-wall temperature profile is symmetric at an initial state. When a gas flows through the sensor tube, the tube-wall temperature difference between the upstream section and the downstream section increases with time and increases with increased mass flow rate. Fig. 10 shows the tube-wall and fluid temperatures along the sensor tube at a transient state for a typical run. There is no difference between the tube wall temperature and the fluid temperature at zero flow. When the fluid flows, the tube temperature becomes higher than the fluid temperature in the upstream section and lower than the fluid temperature in the downstream section. From Fig. 10, the transient heat transfer mechanism in the sensor tube can be explained as follows. Because of the heater wire wound at the center portion of the sensor tube, the sensor tube

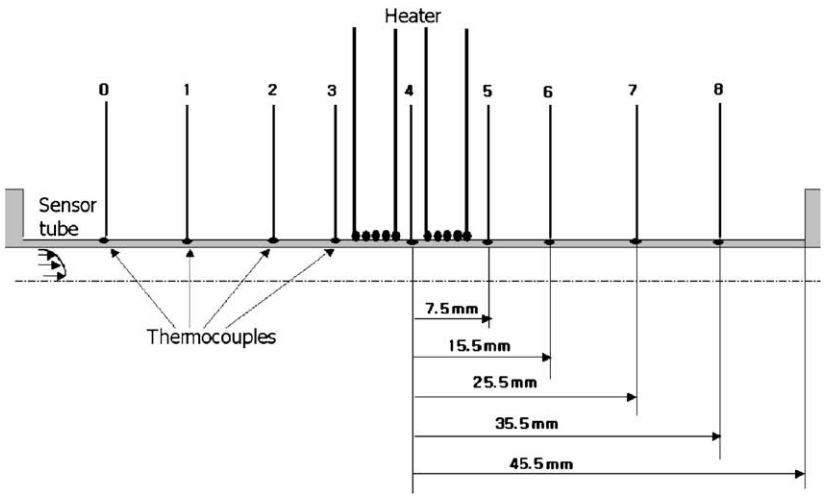

Fig. 7. Positions of the heater and thermocouples.

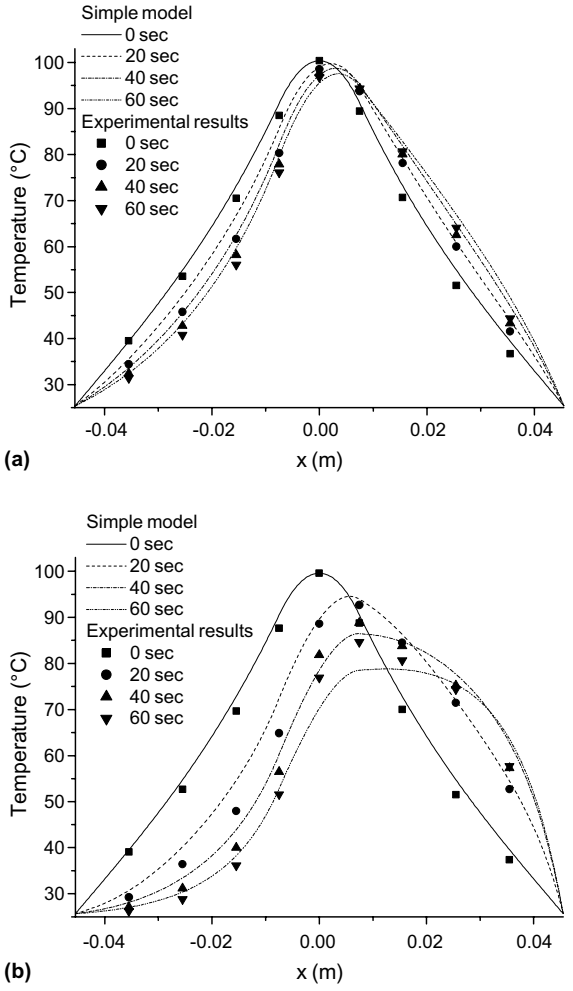

Fig. 8. Comparison between tube-wall temperature profiles using the simple numerical model and experimental results for an outer diameter of 0.8 mm. (a) Flow rate of 10 SCCM. (b) Flow rate of 30 SCCM.

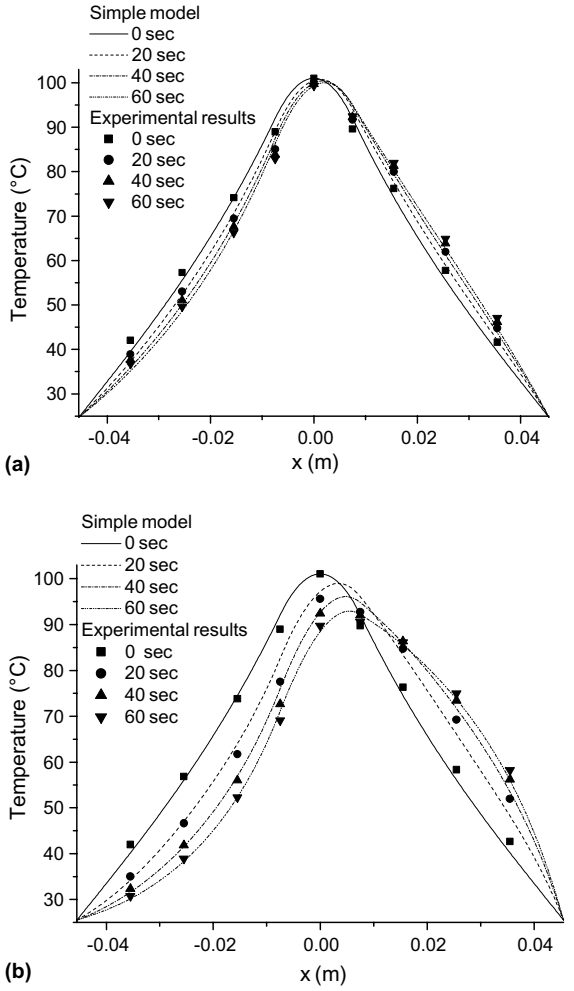

Fig. 9. Comparison between tube-wall temperature profiles using the simple numerical model and experimental results for an outer diameter of 1.2 mm. (a) Flow rate of 10 SCCM. (b) Flow rate of 30 SCCM.

temperature is higher than the ambient fluid temperature at the inlet. Thus, when fluid flows into the upstream section of the sensor tube, heat is transferred from the tube to the fluid by convection in the upstream section. The fluid heated along the upstream section of the sensor tube flows into the downstream section. This fluid has a higher temperature than the tube in the downstream section. So, heat transfer from the fluid to the tube occurs along the downstream section of the sensor tube. Consequently, heat is transferred from the tube wall along the upstream section and conversely to the tube wall along the downstream section. Therefore, as time progresses, the temperature in the upstream section of the tube decreases and the temperature in the downstream section increases. Finally, the temperature of the sensor tube reaches its equilibrium profile when

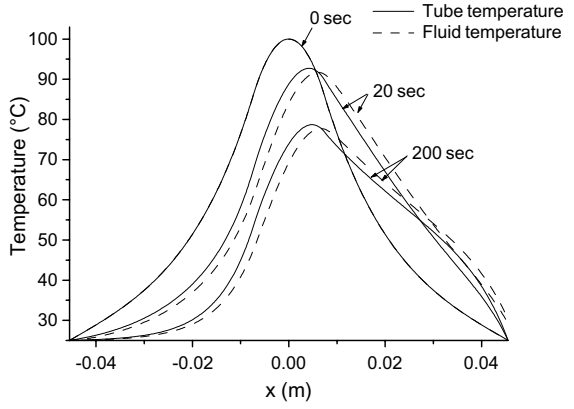

Fig. 10. Typical tube temperature and fluid temperature along the sensor tube at a transient state.

there exists a balance among heat generation, flow convection, axial conduction and heat loss.

5. Correlation for the response time

5.1. Response time of the sensor tube

The response time of the sensor tube can be expressed in many different ways. For example, it can be defined as the time required for the sensor tube to reach 63.2% of the steady-state value (time constant). In this paper, the response time of the sensor tube is given as follows.

$$\frac{\overline{T}_t(-L_s, t_{resp}) - \overline{T}_t(L_s, t_{resp})}{\overline{T}_t(-L_s, t_{final}) - \overline{T}_t(L_s, t_{final})} = 0.95 \tag{18}$$

where t_{final}, t_{resp}, and L_s are the time when the temperature of the sensor tube reaches its final steady-state value, response time of the sensor tube, and distance from the center of the sensor tube to the center of a temperature-sensitive wire, respectively. In other words, the response time is defined as a time interval from the moment that the fluid begins to flow to the moment that the temperature difference reaches 95% of the temperature difference between the upstream and downstream sensors at equilibrium. It is assumed that temperature-sensing wires are symmetrically placed at $x = -L_s$ and $x = L_s$, because the sensors are in general symmetrically located from the heating wire in a TMFM.

5.2. Correlation for the response time

To come up with a correlation for the response time of the sensor tube with the proposed simple numerical model, a functional form of the correlation should be known. For this, we rely on a scale analysis to find a functional form [21]. The functional form of the correlation is determined to be

$$t_{resp} = \frac{\rho_t C_t A_t L}{\left(C_1 \frac{k_t A_t}{L} + C_2 L \frac{1}{R_r}\right)\left(1 + \left(\frac{\dot{m} c_g}{C_3 \frac{k_t A_t}{L} + C_4 L \frac{1}{R_r}}\right)^2\right)} \tag{19}$$

where L is half of the total sensor tube length. We should determine values of coefficients appearing in Eq. (19) to complete the correlation. To obtain these coefficients, we obtain the response time for varying sets of parameters using the proposed simple model. These parameters include the mass flow rate, heat loss, sensor position, heater position, and thermophysical properties. Then, coefficient values that match a variety of different response times are determined using a least square fit [22]. Table 2 shows the results of the coefficient values. We applied the calculated coefficients to the proposed correlation to compare the results of the simple numerical model. As shown in Fig. 11, there are close agreements between the results based on the proposed correlation and the various results of the simple numerical model.

Table 2
Coefficients for the correlation

L_h/L_s	L_s/L	Coefficients			
		C_1	C_2	C_3	C_4
0.25	0.2	3.427	0.4407	1.986	0.2356
	0.4	3.341	0.3349	1.955	0.2268
	0.6	3.352	0.2745	1.927	0.2319
	0.8	3.445	0.2421	1.875	0.2425
0.5	0.2	3.415	0.4382	1.983	0.2344
	0.4	3.35	0.3379	1.961	0.2248
	0.6	3.367	0.2933	1.924	0.2366
	0.8	3.498	0.2846	1.877	0.2483
0.75	0.2	3.411	0.4291	1.986	0.2303
	0.4	3.337	0.3441	1.954	0.2277
	0.6	3.391	0.3203	1.925	0.2404
	0.8	3.571	0.35	1.879	0.2506

The correlation for the sensor-tube response time produced results with a relative error of 30% or less. This correlation for the response time depends on the flow rate, the thermal properties of the sensor tube and the gas, heat loss, sensor tube length (L), sensor tube area, the ratio of heater wire length (L_h) to sensor position length (L_s), and the ratio of sensor position length (L_s) to half of the total tube length (L). Alternatively, we obtained the coefficients of the correlation with the experimental results. The coefficients that fit the experi-

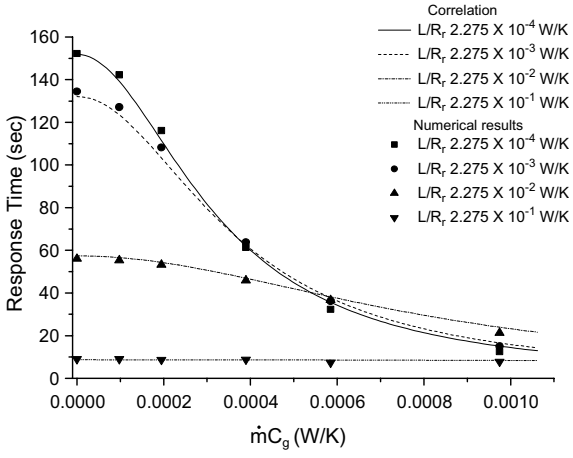

Fig. 11. Comparison between response times using the correlation and using the simple numerical model ($L_h/L_s = 0.5$, $L_s/L = 0.2$, $\rho_t C_t A_t L = 8.243 \times 10^{-2}$ J/K, $k_t A_t/L = 1.609 \times 10^{-4}$ W/K).

mental data are determined to be as follows: $C_1 = 3.00$, $C_2 = 0.71$, $C_3 = 3.83$, $C_4 = -0.141$. The correlation based on the experimental results can be applicable for the range of Eq. (20).

$$0.4 < \frac{k_t A_t R_r}{L^2} < 0.7 \tag{20}$$

The correlation based on the analytical model and the correlation based on the experimental results compare favorably with the experimental results. Fig. 12 shows the relationship between the mass flow rate and the response time using the correlation based on the proposed simple model, the correlation based on the experimental results, and the experimental results. The precision error shown in Fig. 12 is associated with a 95% confidence level. The correlation from the simple model and the correlation from the experimental results predict the experimental results to within a relative error of 30% and 10%, respectively.

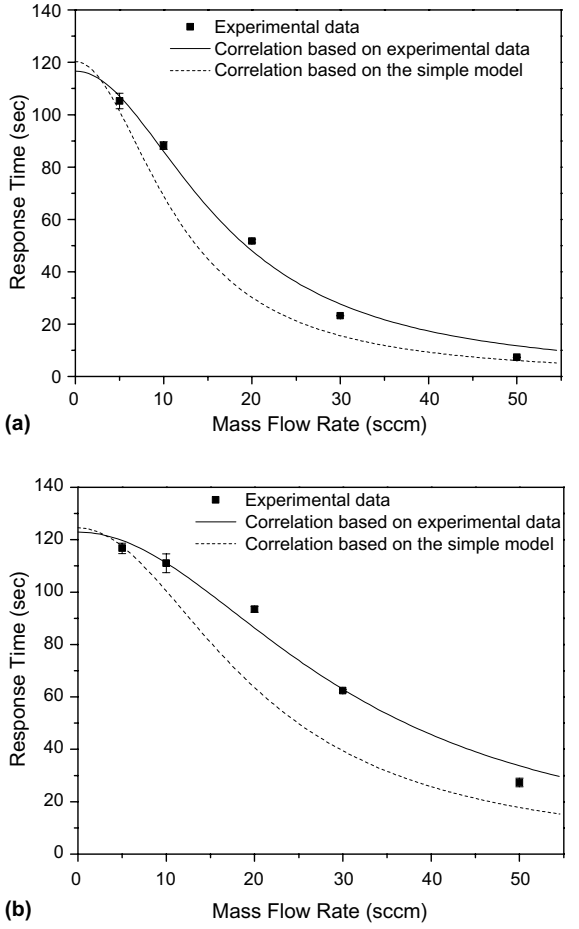

Fig. 12. Comparisons of response times of experimental results and correlations. (a) Outer diameter of 0.8 mm ($D_{out} = 0.812$ mm, $D_{in} = 0.562$ mm, $L_h/L_s = 0.5$, $L_s/L = 0.2$). (b) Outer diameter of 1.2 mm ($D_{out} = 1.257$ mm, $D_{in} = 0.977$ mm, $L_h/L_s = 0.5$, $L_s/L = 0.2$).

We investigate the effects of these parameters on the response time by using the proposed correlation. The following are the characteristics of the sensor-tube response time:

(1) When the mass flow rate is increased, the response time is decreased.
(2) The thermal conductivity of the sensor tube is inversely proportional to the response time.
(3) The density and the heat capacity of the sensor tube are linearly proportional to response time.
(4) Heat loss is closely related to response time. When heat loss is increased, the response time is decreased.
(5) Increased tube length and cross-sectional area increase the response time.
(6) The response time does not greatly depend on the ratio of heater wire length (L_h) to sensor position length (L_s) or the ratio of sensor position length (L_s) to half of the total tube length (L) compared to other parameters.
(7) The response time does not depend strongly on the fluid properties except for the thermal conductivity.

6. Conclusion

In the present paper, a simple numerical model for transient heat transfer phenomena involving the sensor tube of a TMFM is presented. The results of the simple numerical model are verified by experimental results. Based on the results of the simple model, the transient heat transfer mechanism in the sensor tube is explained. A correlation for predicting the response time of the sensor tube is presented using the proposed simple model. This correlation can estimate the response time of the sensor tube quantitatively to within 30% of relative error, under the condition that thermophysical properties of the sensor tube, such as thermal conductivity, density, and heat capacity, are larger than those of fluid. Using the proposed correlation, physical meanings and characteristics of the response time of the sensor tube are presented.

Acknowledgement

The present work was funded by Korea Institute of Science & Technology Evaluation and Planning under grant number 2-578 through the National Research Lab Program. This assistance is greatly appreciated.

References

[1] D.D. Valle, P.A. Tanguy, P.J. Carreau, Characterization of the extensional properties of complex using an orifice flowmeter, J. Non-Newtonian Fluid Mech. 94 (2000) 1–13.

[2] M.P. Henry et al., A self-validating digital coriolis mass flow meter: an overview, Control Eng. Pract. 8 (5) (2000) 487–506.

[3] N.T. Nguyen, Micromachined flow sensors—a review, Flow Meas. Instrum. 8 (1) (1997) 7–16.

[4] A. Rasmussen et al., Simulation and optimization of a microfluidic flow sensor, Sensor. Actuat. A 88 (2001) 121–132.

[5] S.A. Tison, A critical evaluation of thermal mass flow meters, J. Vac. Sci. Technol. A 14 (4) (1996) 2582–2591.

[6] P. Rudent, P. Navratil, Design of a new sensor for mass flow controller using thin-film technology based on an analytic thermal model, J. Vac. Sci. Technol. A 16 (6) (1998) 3559–3563.

[7] A.E. Widmer, R. Fehlmann, W. Rehwald, A calibration system for calorimeter mass flow device, J. Phys. E: Sci. Instrum. 15 (1982) 213–220.

[8] Mariano, F. Charles, U.S. Patent No. 4548075, 1985.

[9] J.H. Ewing, F.G. Ramberg, U.S. Patent No. 4464932, 1984.

[10] K. Tujimura, O. Akebe, K. Satoh, U.S. Patent No. 4815280, 1987.

[11] L.D. Hinkle, C.F. Mariano, Toward understanding the fundamental mechanisms and properties of the thermal mass flow controller, J. Vac. Sci. Technol. A 9 (3) (1991) 2043–2047.

[12] K. Komiya, F. Higuchi, K. Ohtani, Characteristics of a thermal gas flowmeter, Rev. Sci. Instrum. 59 (3) (1998) 477–479.

[13] S.J. Kim, S.P. Jang, Experimental and numerical analysis of heat transfer phenomena in a sensor tube of a mass flow meter, Int. J. Heat Mass Transfer 44 (2001) 1711–1724.

[14] M. Viswanathan, A. Kandaswamy, S.K. Sreekala, K.V. Sajna, Development, modeling and certain investigations on the thermal mass flow meters, Flow Meas. Instrum. 12 (2002) 353–360.

[15] K. Toda, C. Maeda, I. Sanemasa, K. Ishikawa, N. Kimura, Characteristics of a thermal mass-flow sensor in vacuum systems, Sensor. Actuator. A 69 (1993) 62–67.

[16] W.M. Kays, M.E. Crawford, Convective Heat and Mass Transfer, third ed., McGraw-Hill, New York, 1993 (Chapter 7).

[17] S.V. Patankar, Numerical Heat Transfer and Fluid Flow, Hemisphere Publishing Corp., New York, 1980, pp. 102–104.

[18] D.W. Peaceman, H.H. Rachford, The numerical solution of parabolic and elliptic differential equations, J. Soc. Ind. Appl. Math. 3 (1955) 28.

[19] H. Robert, Visual Programming with HP VEE, second ed., Prentice Hall, New Jersey, 1997.

[20] T.G. Beckwith, R.D. Marangoni, J.H. Lienhard, Mechanical Measurements, fifth ed., Addison-Wesley Publishing Company, New York, 1993 (Chapter 3).

[21] A. Bejan, Convective Heat Transfer, second ed., Wiley, New York, 1995, pp. 18–21.

[22] J. Dragan, K. Gordana, S. Rudolf, Least squares fitting gompertz curve, J. Comp. Appl. Math. 169 (2004) 359–375.